PAPER

Pitcher plant-bioinspired bubble slippery surface fabricated by femtosecond laser for buoyancy-driven bubble self-transport and efficient gas capture†

Yunlong Jiao, [ID] ‡[a] Xiaodong Lv,‡[b] Yiyuan Zhang,[a] Chuanzong Li,[a] Jiawen Li,*[a] Hao Wu,[a] Yi Xiao,[c] Sizhu Wu,[b] Yanlei Hu,[a] Dong Wu [ID] *[a] and Jiaru Chu[a]

Functional materials with specific bubble wettability play an important role in manipulating the behavior of underwater gas bubbles. Inspired by the natural Pitcher plant, we designed a large area lubricated slippery surface (LSS) by femtosecond laser processing for buoyancy-driven bubble self-transport and efficient gas capture. The mechanism of bubble self-transport involves a competition between the buoyancy and the resistance due to drag force and hysteresis. The transportation velocity of the bubbles on the LSS is strongly associated with the surface tension of the lubricants. The lower the surface tension, the higher the sliding velocity. On the basis of sufficient bubble adhesion, the shaped LSS tracks are fabricated to guide the bubble movement and achieve continuous manipulation between bubble merging and detachment. We demonstrate that these designable pathways on the LSS not only manipulate bubble behavior in a two-dimensional space but also realize three-dimensional movement of bubbles on the Mobius-striped LSS. Finally, a gas catcher decorated with large area LSS is manufactured for underwater bubble capture, which maintains a high capture efficiency (more than 90%) with an air output of ~3.4 L min^{-1}. This finding reveals a meaningful interaction between the underwater bubbles and the LSS surface, accelerating the applications of bubble slippery surfaces in underwater flammable gas collection and tail gas treatment.

1 Introduction

The directional transportation of underwater air bubbles has significant applications in a wide variety of fields from science to industries,[1–10] such as in catalytic reactions,[1–3] wastewater treatment,[4,5] and generation of electrochemical H_2.[6] Nature-inspired functional surfaces with specific wettability have been developed as useful tools for controlling the movement of small bubbles.[11–15] For instance, the lotus leaf provided a unique strategy for constructing a multiscale micro/nano-structured surface with super-hydrophobicity, which shows high adhesion towards air bubbles in liquids and excellent bubble-capturing abilities, enabling the collection of useful energy-rich gases from the deep sea.[11] The back of Namib desert beetles together with the pitcher plant has inspired the design of nanoporous lubricated surfaces for underwater on-demand bubble transportation.[12] Additionally, a large number of researches have attempted to reveal the mechanism of controlling the movements of underwater bubbles and directional manipulation on the basis of bio-inspired surfaces.[16,17] In general, the super-hydrophobic surfaces provide a strong adhesive force towards bubbles in liquid environments,[18] but the stronger adhesion between gas and multiscale micro/nanostructures hinders the detachment of bubbles from the substrate. When the bubble comes into contact with the super-hydrophobic surface, it spreads rapidly due to the interaction between the air and the surface.[19,20] Additionally, the bubble ceases to move freely under buoyancy for further directional transportation due to the high adhesion between the gas and the super-hydrophobic surface.

Inspired by the Pitcher plant, researchers have studied lubricated slippery surfaces that exhibit excellent ability of controlling bubble motions due to buoyant force and Laplace driven force.[12,18,21] For example, Zhang *et al.*[21] designed a tapered slippery surface on the basis of two biomimetic principles (the cactus and the Pitcher plant) to achieve directional

[a]CAS Key Laboratory of Mechanical Behavior and Design of Materials, Department of Precision Machinery and Precision Instrumentation, University of Science and Technology of China, Hefei 230026, China. E-mail: dongwu@ustc.edu.cn, jwl@ustc.edu.cn

[b]School of Instrument Science and Opto-electronics Engineering, Hefei University of Technology, Hefei, 230009, China

[c]School of Mechanical Engineering, Nantong Vocational University, Nantong, 226007, China

†Electronic supplementary information (ESI) available. See DOI: 10.1039/c8nr09348b

‡These authors contributed equally to this work.

and continuous bubble transport in a liquid; however, the fabrication process was complex and the bubble transportation was restricted by the size of the tapered area. Wang *et al.*[12] fabricated a lubricated surface inspired by the back of the desert beetle, which involved intertwined hydrophilic/hydrophobic regions. Due to the high affinity and low resistance to movement between the bubbles and the lubricated surface, the movement of the bubbles could be easily controlled in the pre-designed tracks for further on-demand gas collection. Moreover, Pei *et al.*[22] prepared an underwater unidirectional penetration film for gas separation by modifying copper meshes, which was named as "bubble diode". In short, despite great progress in the studies on bioinspired slippery surfaces, current preparation processes of slippery surfaces are easily susceptible to external influences and the chemical solvents often cause environmental pollution. It is still a challenge to find a facile way to rapidly fabricate large area slippery surface and easily manipulate bubble behavior. In addition, further research is needed to achieve progressive practical applications. For example, the influence of the lubricant surface tension, viscosity and bubble volume on the sliding velocity and bubble contact angle, the manipulation of bubbles in a

three-dimensional space and the mechanism of bubble interaction with slippery surfaces should be further studied.

Herein, we prepared a grooved structure on an aluminium surface by the femtosecond laser direct writing technology. The LSS was then obtained through super-hydrophobic treatment and lubrication process. The obtained LSS showed an excellent ability for manipulating underwater bubbles with the assistance of buoyancy and was suitable to be used in a variety of liquid environments, such as acidic and alkaline. We analyzed the influence of the bubble volume on the bubble contact angle (BCA) and the bubble sliding angle (BSA). It is worth noting that the variations in BCA and BSA have close relationship with the kind of lubricants used. Additionally, we investigated the influence of lubricant surface tension, viscosity and bubble volume on the bubble sliding velocity. In order to show the excellent ability of controlling the bubble motion, we designed different shapes of tracks on the LSS and demonstrated the efficient control of bubble movement in both two-dimensional and three-dimensional spaces, which largely increases their potential applications. Finally, we fabricated a detector-like gas catcher covered by a large LSS for underwater gas capture with high capture efficiency.
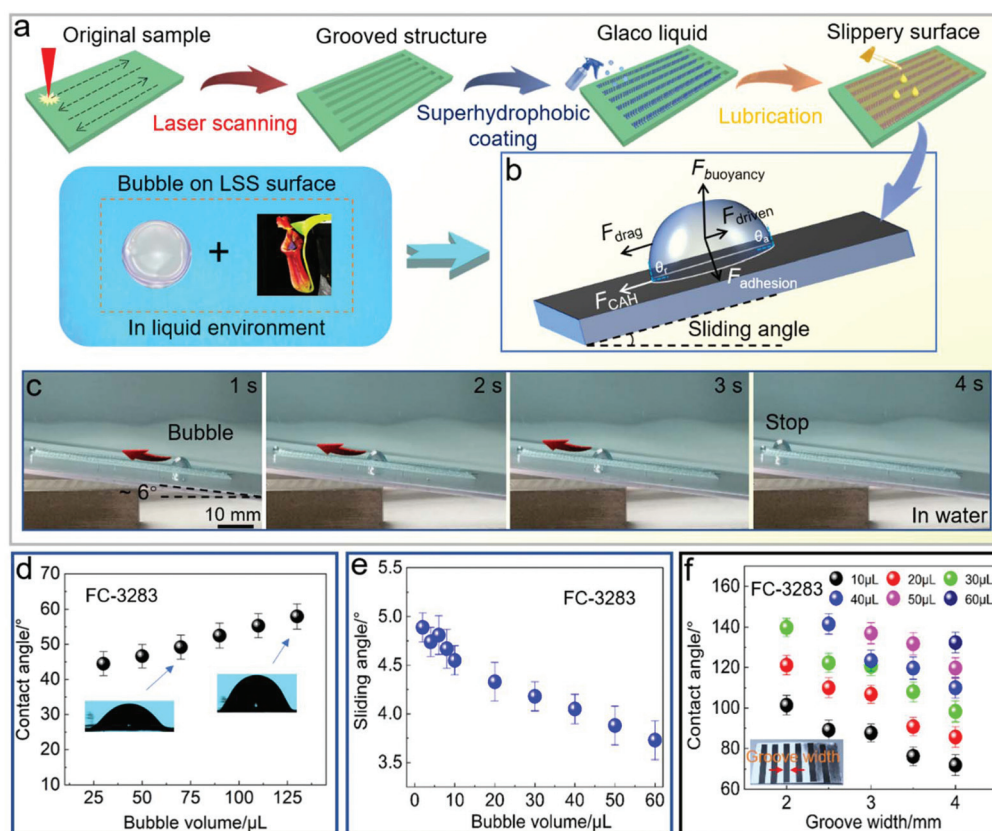

Fig. 1 Overview of LSS fabrication and its application to bubble transportation based on buoyancy. (a) The detailed LSS preparation process inspired by the Pitcher plant, including three main steps of laser scanning, super-hydrophobic coating and lubrication. (b) The mechanical analysis of a bubble when it slips along the inclined LSS. (c) The sliding process of the bubble on the inclined LSS from a side view. (d) The relationship between the bubble volume and BCA. (e) The relationship between the bubble volume and BSA. (f) The influence of the groove width on the BCA under different bubble volumes.

2 Results and discussion

Fig. 1a shows a schematic of the LSS preparation process inspired from the Nepenthes pitcher plants. We integrated liquids into rough material surfaces to imitate the performance of the pitcher plant. Three engineering criteria must be satisfied to create a stable liquid-infused surface.[23] First, the lubricant liquid must be wet and stably adhere to the substrate. Second, the substrate must prefer the lubricant liquid compared to water. Third, the lubricant and the test liquid must be immiscible. To meet the above criteria, the rough grooved structure was processed on an aluminium alloy sheet by femtosecond laser ablation (Fig. 1a and Fig. S1†). The grooves were regularly distributed on the ablated surface, and some micro/nanoparticles appeared on the grooves (Fig. S2b†). Then, the Glaco solvent was evenly sprayed on the surface to reduce the surface energy to make the laser-induced sample super-hydrophobic. Subsequently, the lubricant FC-3283 was dripped onto the super-hydrophobic surface. It would enter the microstructure and spread rapidly on the surface due to

the capillary force. In order to obtain a uniform lubricant film, the sample was processed by spin coating for 5 min. Due to the low surface energy, the lubricant maintained its stability under water. The prepared slippery surface was capable of underwater bubble self-transport due to buoyancy effects (Fig. 1b). An approximate 10 μL bubble moved 4 cm on the slippery area (5 mm wide) with a sliding angle of ~6° in 4 seconds (Fig. 1c). The mechanical model of the bubble slipping upward along the slippery surface is shown in Fig. 1b. The axis-directional component of the buoyancy gives the bubble its main driving force. This force can be calculated as $F_{driven} = F_{buoyancy}·\sin\theta$ (θ denotes the sliding angle), where $F_{buoyancy}$ can be calculated using the equation $F_{buoyancy} = \rho·g·V$ (ρ, g and V denote the water density, gravitational acceleration, and the bubble volume, respectively). The adhesion force ensures the bubble's interaction with the LSS, which is balanced by the buoyancy component perpendicular to the axial direction.[18] The sliding behavior resistance (F_{resist}) is composed of the resistance of contact angle hysteresis (F_{CAH}) and the drag force (F_{drag}).[18] The resistance of CAH can be
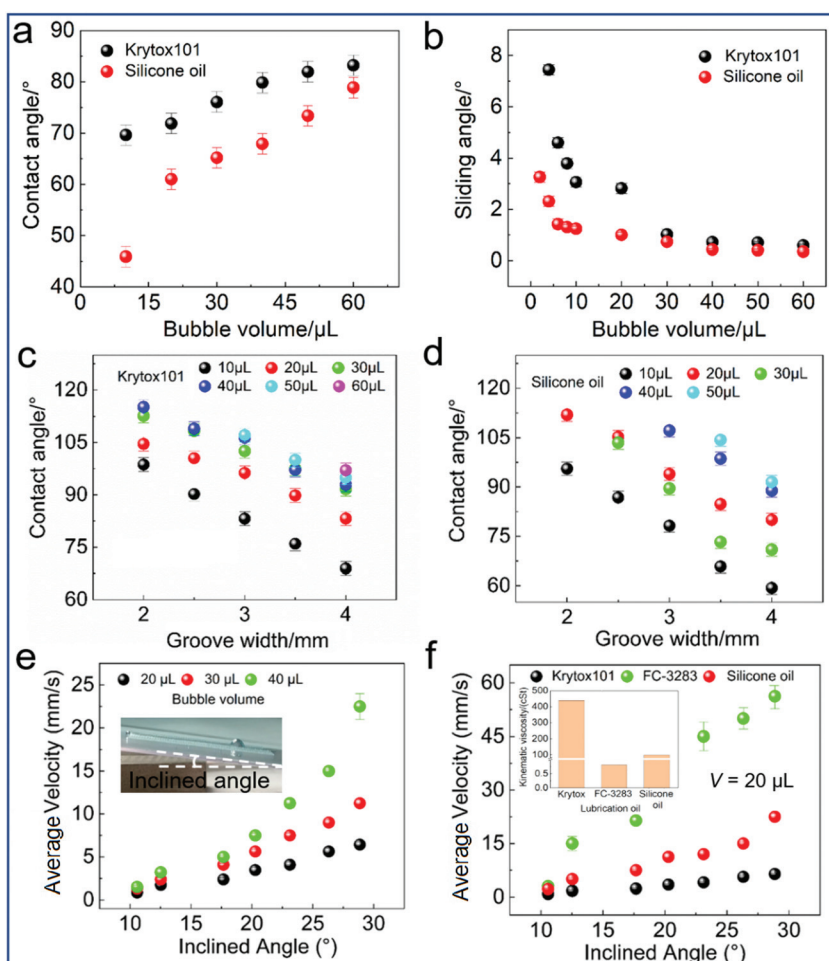

Fig. 2 Quantitative research of BCA, BSA and sliding velocity on the LSS with different lubricants. (a) (b) The influence of the lubricant type on the BCA and BSA, respectively. (c) The relationship between the groove width and BCA on the LSS with different lubricants. (e) The influence of bubble volume on the average velocity with the increase in the inclined angle. (f) The influence of lubricant type on the average velocity with the increase in the inclined angle.

expressed as follows: $F_{CAH} = \gamma \cdot L \cdot (\cos\theta_r - \cos\theta_a)$, where γ is the surface tension of the lubricant, L is the line length along the axis-direction between the bubble and the surface, and θ_r and θ_a represent the advancing and receding angles of the bubble, respectively. The drag force is mainly related to the velocity of the bubble.[24,25] When the F_{driven} exceeds the F_{resist}, the bubble freely slides along the slippery area. In aqueous environments, the BCA increases linearly with the increase in the bubble volume from 30 μL to 130 μL (Fig. 1d), which is mainly due to the influence of the buoyancy during BCA measurements. Furthermore, the relationship between the bubble volume and sliding angle was investigated. A 2 μL bubble slid upward with a sliding angle of 5°, and the sliding angle decreased to 3.5° when the bubble volume increased to 60 μL (Fig. 1e). Finally, the BCAs on the slippery area with different widths were researched (Fig. 1f). The groove width was defined as the boundary of the LSS so the bubble could only slide along the laser-induced area (Fig. S2†). The results show that the BCA apparently decreases when the groove width increases from 2 mm to 4 mm. A bubble with a certain volume tends to spread freely on the slippery area if the LSS has no boundary restriction. As the groove width is small, the LSS boundary restricts the spreading of the bubble along the vertical direction when the bubble volume increases, which contributes to the increase in the BCA; finally, the enlarged bubble detaches from the LSS because the buoyancy exceeds the adhesive force.

We also conducted a series of BCA and BSA experiments on the LSS with different lubricants, such as silicone oil and Krytox 101 (Fig. 2). The BCAs on the LSS with different lubri-cants increased with the increase in the bubble volume. However, the BCA on different LSS with the same bubble volume showed significant differences, which were mainly due to the variation in surface tensions of the lubricants. According to Young's wetting theory,[26,27] the liquid tends to wet the substrate with high surface energy and shows a smaller liquid contact angle. Similarly, when the substrate is lubricated by oil, the solid–liquid interaction changes due to the oil-liquid interaction. Therefore, the liquid tends to spread on the lubricant with high surface tension. In contrast, when the same substrate is placed in water, the gas contact angle increases with the increase in the surface tension of the lubri-cant, which agrees with the experimental result shown in Fig. 2a. Additionally, the variation of BCA on different lubri-cated surfaces is closely related to the surface tension of the lubricants. In general, the resistance of CAH determines whether the bubble begins to move on the surface. As the surface tension of silicone oil is lower than that of the Krytox 101(Table S1†), the CAH resistance for the same bubble volume decreases, which contributes to a smaller BCA on the LSS with silicone oil (Fig. 2b). To investigate the influence of the groove width on the BCA, the BCAs were measured with widths ranging from 2 to 4 mm (Fig. 2c and d). The results show that the BCA apparently decreases when the groove width increases from 2 mm to 4 mm at different bubble volumes. For example, the contact angle of a 10 μL bubble gradually decreases from 95° to 60° on the LSS with silicone oil (Fig. 2d). When the groove width is small, the boundary of the slippery area restricts the spreading of the bubble, which contributes to the increase in the bubble contact angle. Finally, the bubble
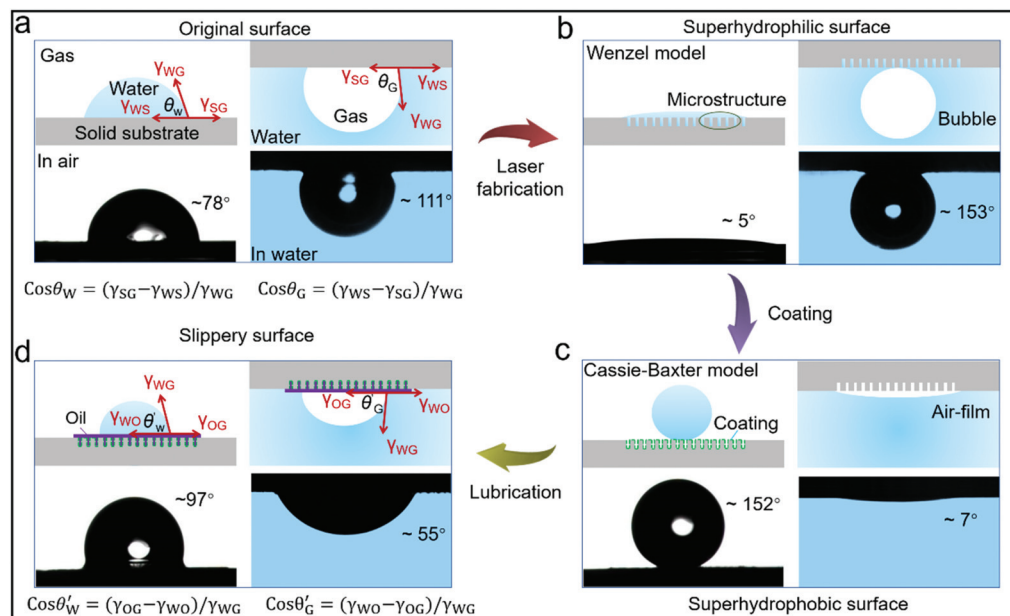

Fig. 3 Different wetting states in LSS fabrication. (a) The original surface is hydrophilic and underwater aerophobic. (b) After laser fabrication, the structured surface shows super-hydrophilicity and underwater super-aerophobicity. (c) The super-hydrophobic treatment makes the sample super-hydrophobic, which belongs to the Cassie-Baxter model. (d) When the lubricant oil is coated on the super-hydrophobic sample, the solid−liquid interaction is impacted by the liquid-lubricant interaction, which contributes to the variation of water contact angle and BCA.

detaches from the substrate when the buoyancy exceeds the adhesive force between the bubble and the lubricant.

As mentioned in the above formulas, the driving force and resistance are primarily affected by the bubble volume, surface tension and viscosity of the lubricant. The sliding velocities of the samples with varying inclined angles were measured and is shown in Fig. 2e and f. As the inclined angle increased from 10° to 28°, the average velocity of a 20 μL bubble increased from 0.87 mm s^{-1} to 6.43 mm s^{-1}. A 20 μL bubble can reach up to 56.25 mm s^{-1} on the FC3283-infused surface while the velocity of the bubble on the silicone oil-infused surface is as low as 22 mm s^{-1}. The results show that the bubbles slide faster on the LSS with lower viscosity lubricants (Fig. 2f), which is mainly caused by the variation in CAH resistance due to the differences in the lubricant surface tensions (Table S1†). Under the same bubble volume, the resistance of CAH plays a dominant role in determining the sliding velocity of the bubble. A lower surface tension correlates with a decreased CAH resistance, so the bubble slides faster on the lubricant with a small surface tension.

In order to study the variation in surface wettability during the LSS fabrication process, the contact angles were measured and the physical mechanism was analyzed (Fig. 3). On the orig-inal unprocessed aluminium metal (Fig. 3a), hydrophilicity was observed with a water contact angle (WCA) of ~78° and aerophobicity with a BCA of ~111°. After laser ablation, the processed area was full of rough micro/nanostructures, which showed super-hydrophilicity with a WCA of ~5° and under-water super-aerophobicity with a BCA of ~153° (Fig. 3b). Then, a chemical reagent of low surface energy was sprayed onto the uneven surface in order to show super-hydrophobicity with a WCA of ~152° and underwater super-aerophilicity with a WCA of ~7° (Fig. 3c). Finally, the super-hydrophobic sample was coated with a lubricant, which showed a WCA of ~97° and a BCA of ~55° (Fig. 3d). It is worth noting that the solid–liquid interaction was occupied by the lubricant-liquid interaction on the LSS. When a droplet was applied to the LSS, it directly con-tacted the infused lubricant and not the solid. As shown in Fig. 3d, the water contact angle can be expressed as follows:

$$\text{Cos } \theta'_{W} = (\gamma_{OG} - \gamma_{WO})/\gamma_{WG} \tag{1}$$

where γ_{OG} is the surface tension of the lubricant oil, γ_{WO} is the surface tension between oil and water, and γ_{WG} is the surface tension of water. When the same substrate is placed under
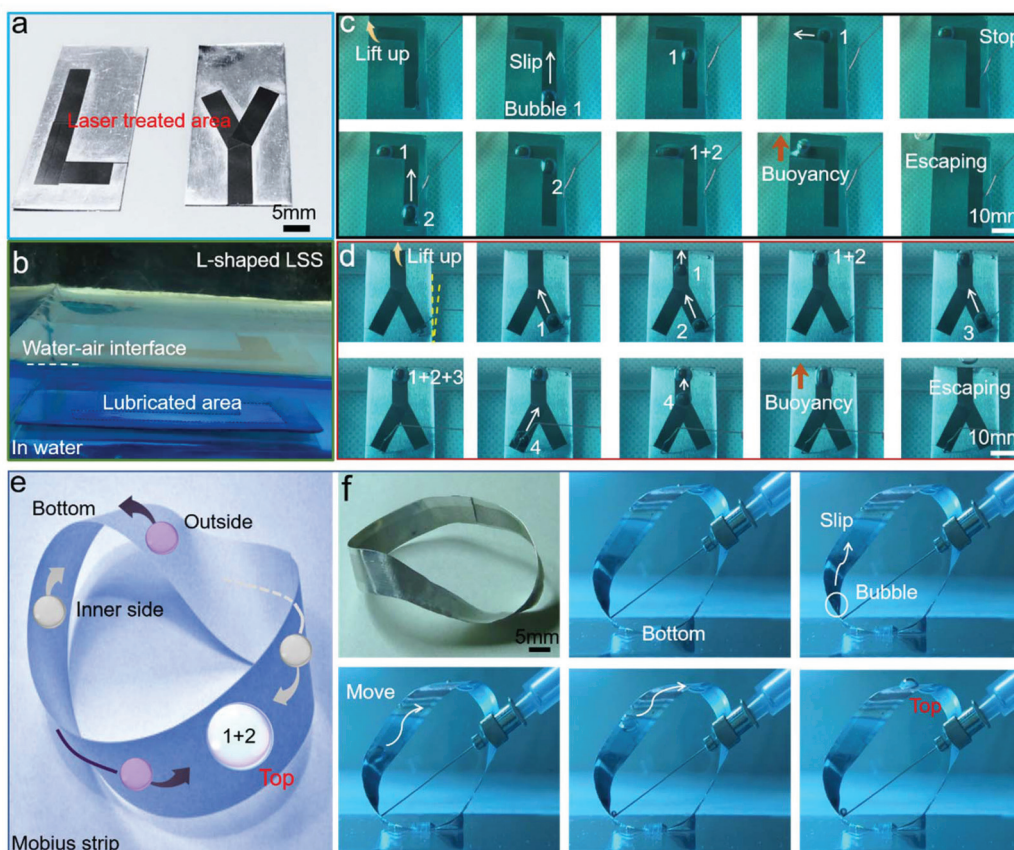

Fig. 4 The bubble transport on the shaped LSS tracks in both two-dimensional and three-dimensional spaces. (a) A digital photo of L-shaped and Y-shaped LSS tracks. (b) When the L-shaped LSS is placed in water, the slippery area shines due to the existence of lubricant oil. (c) (d) Continuous bubble transport on the L-shaped and Y-shaped LSS tracks. (e) Sketch of bubble transport on the Mobius strip-shaped LSS. (f) The detailed bubble transport process on the Mobius strip-shaped LSS in a three-dimensional space.

water (Fig. 2d), the gas contact angle on the original surface can be expressed as follows:

$$\cos \theta'_G = (\gamma_{WO} - \gamma_{OG})/\gamma_{WG} \qquad (2)$$

It can be calculated from eqn (1) and (2) that θ'_W and θ'_G meet the following relationship:

$$\theta'_G = 180° - \theta'_W \qquad (3)$$

It is worth noting that the slippery surface with lubricated oils modified the original contact among solid, liquid and air. The interaction between the liquid and the lubricant plays a dominant role in determining the attachment and the movement of the droplet in air or the bubble in liquid.[28] According to eqn (3), the hydrophobic substrate will be aerophilic in an aqueous medium on the LSS, while the hydrophilic substrate will be aerophobic.

In order to show the continuous process of bubble transport on the LSS driven by buoyancy, two kinds of LSS tracks, namely, L-shaped and Y-shaped tracks, were designed and fabricated by laser ablation (Fig. 4a). When the as-prepared sample was placed in water, the slippery area shined as it was coated with lubricant oil (Fig. 4b). In the liquid environment, the bubble moved upward along the smooth L-shaped path successfully by lifting up the top left corner of the sample (Fig. 4c and Movie S1†). Bubble 1 stopped at the end of the

track due to the strong adhesion between the bubble and the lubricant. Then, bubble 2 slipped along the track and merged with bubble 1 at the end of the track. Finally, the merged bubble deviated from the track, as the buoyancy was higher than the adhesive force. Additionally, the merging of the two bubbles on a Y-shaped track was explored for the potential application in a gas-mixing microfluidic device (Fig. 4d and Movie S2†). The bubbles were respectively added on the two sides of the Y-shaped track, and they merged at the end of the track due to buoyancy. With the continuous merging of bubbles, the merged bubble finally escapes from the track. Finally, a Mobius striped LSS was fabricated to display the self-transport of bubbles in a three-dimensional space (Fig. 4e–f). Fig. 4e shows a sketch of the bubbles slipping on the Mobius strip. Two bubbles were released at the bottom of the strip, and they respectively slid upward from both the sides of the strip. Finally, they gathered at the same side of the strip and merged into a large bubble. The detailed process is displayed in Fig. 4f and Movie S3.† In short, these functional LSS tracks with specific paths show possibilities for potential applications.

Underwater bubble capture and gas collection has been highly desirable in recent studies. Although this has been researched using different kinds of materials with superwettability, it remains a challenge to achieve high efficiency bubble
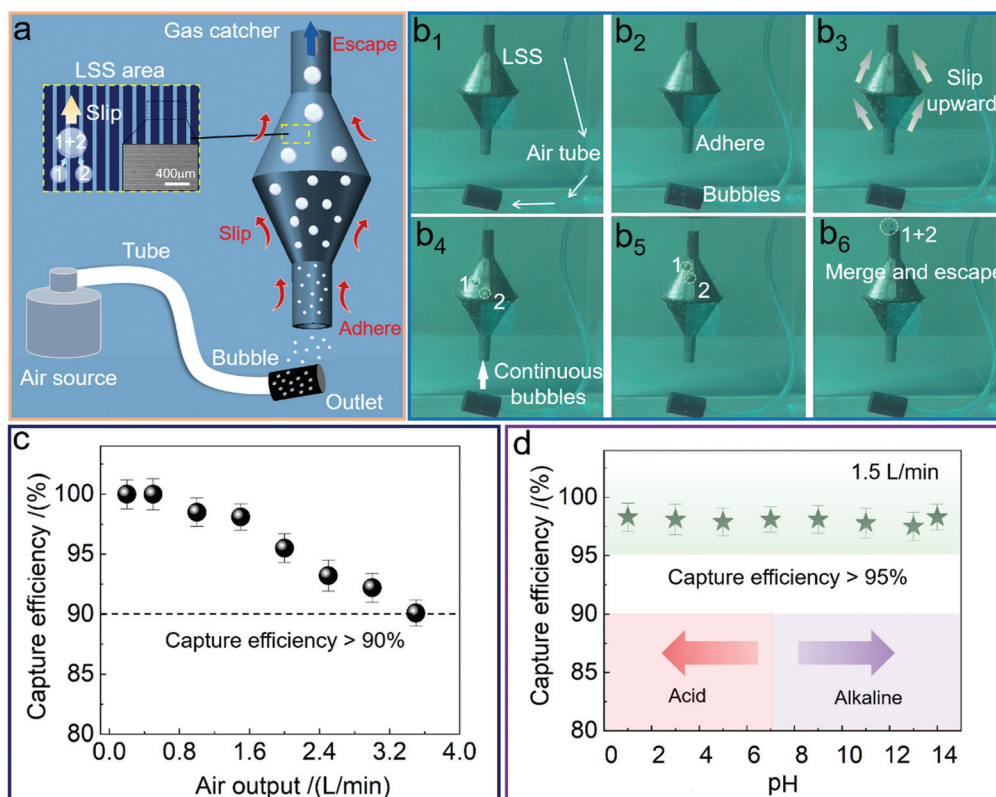

Fig. 5 A funnel-like gas catcher coated with a large area of LSS outside for rapid and efficient bubble capture. (a) The mechanism of bubble capture using the gas catcher. (b) Continuous photos of bubbles captured in liquid. (c) The relationship between the capture efficiency and air output. (d) The relationship between the capture efficiency and pH with an air output of 1.5 L min^{-1}.

capture on a large-area LSS. Additionally, the multiscale-structured surfaces with superwettability are usually unstable due to influences of the external environment, such as high temperature and pressure, which seriously affect the efficiency of capturing bubbles. Therefore, the large-area LSS was investigated for rapid bubble capture (Fig. 5). The three-dimensional model of an underwater gas catcher is shown in Fig. 5a, and it can be seen that the detector-like gas catcher is composed of two funnel-like components coated with large-area LSS outside. The detailed process of bubble capture and transportation is divided into three steps (Fig. 5b). The smaller bubbles from the air source first adhere to the lower side of the catcher (Fig. 5b$_2$) and then slip rapidly along the LSS area due to buoyancy (Fig. 5b$_3$). During the process of the bubbles slipping upward on the gas catcher, the velocities of the bubbles with different volumes vary due to the differences in buoyancy. When the bubbles with different velocities meet at some position on the LSS, they merge into a single larger bubble formed by the interaction between the two air bubbles. With the continuous release of bubbles from the air outlet (Fig. 5b$_4$), many smaller bubbles merge with each other (Fig. 5b$_5$). Finally, a large number of merged bubbles escape from the gas catcher and are recollected by another gas catcher. It is worth noting that the funnel-like gas catcher can increase the contact area between the bubble and the surface, which improves the capture efficiency. Fig. 5c schematically depicts the relationship between the air output and the capture efficiency. The decrease in the capture efficiency at higher air outputs is mainly caused by an increase in the escaping bubbles. With the increase in air output, some bubbles may escape from other places and would not adhere to the gas catcher due to the restriction of the LSS area, which decreases the capture efficiency. The gas catcher maintains a capture efficiency (more than 90%) with an increase in the air output from 0.2 L min^{-1} to 3.4 L min^{-1}, which shows its high stability. Additionally, the gas catcher is suitable for different kinds of liquid environments, such as acidic and alkaline conditions (Fig. 5d). The capture efficiency remains as high as ~98% under an air output of ~1.5 L min^{-1}. After placing the gas catcher in air for several days, it maintains a high capture efficiency of more than 95%, which shows its great fatigue stability (Fig. S3†). In short, the proposed funnel-like model with a large-area LSS shows highly efficient bubble capture and may open a new avenue for underwater flammable gas collection system.

3   Conclusion

In summary, inspired by the unique lubricant features of Pitcher plants, we fabricated a multiscale grooved surface by direct femtosecond laser scanning, and the lubricated slippery surface was obtained by super-hydrophobic and lubrication treatments. The LSS shows an excellent ability for manipulating underwater bubbles with assistance of buoyancy and is suitable in a variety of liquid environments, such as acidic and alkaline. The type of lubricant strongly affects the BCA, BSA

and the bubble sliding velocity, mainly due to the variation in the surface tensions of the lubricants. The solid–liquid interaction is impacted by the lubricant–liquid interaction on the LSS, which affects the bubble movement. Additionally, we designed different shapes of tracks on the LSS and showed the efficient control on the movement of the bubbles in both two-dimensional and three-dimensional spaces, which largely increases their potential applications. Finally, we manufactured a detector-like gas catcher covered by a large area LSS for underwater bubble capture, which demonstrates high capture efficiency (more than 95%) after placing in air for several days. The gas catcher could serve as a part of gas collection system with broad potential applications.

4   Experimental details

Materials

6061 alloy sheets (0.2 mm thick) and aluminium foil (20 μm thick) were purchased from New Metal Material Tech. Co., Ltd, Beijing, China. A kind of silane hydrophobic agent (Glaco) was used for the super-hydrophobic treatment, which is an alcohol based dispersion with silica nanoparticles (~40 nm). Three lubricants, including fluorinert (FC-3283), silicone oil and DuPont oil (Krytox 101), were used for the preparation of LSS. The distilled water and NPT (normal pressure and temperature) air were used for contact angle measurements.

Femtosecond laser fabrication

The grooved structure on the sample was achieved by line-by-line laser ablation. The laser beam (104 fs, 1 kHz, 800 nm) from a regenerative amplified Ti : sapphire femtosecond laser system (Legend Elite-1K-HE, Coherent, USA) was employed for ablation. The laser power, scanning spacing and speed were set at 300 mW, 100 μm and 1 mm s^{-1}, respectively. Additionally, the differently shaped LSS tracks were achieved by joining the fabricated area.

Characterization

The micro/nanostructure ablated by laser was characterized using a field-emission scanning electron microscope (JSM-6700F, Japan). The contact angle of the water and bubbles were measured under 10% humidity and 20 °C temperature.

Self-transport of bubbles on the LSS

The as-prepared samples were placed under liquid in a rectangular transparent box. We used an injector to add bubbles onto the LSS. By controlling the inclined angle of the samples, the bubbles slid along the designed shaped tracks due to buoyancy. The detailed movements were recorded by a digital camera.

Statement of contributions

D. W. and J. W. L. participated in the design of this study, and they both performed the statistical analysis. Y. L. J. and

X. D. L. conducted the experiments and prepared the manuscript. Y. Y. Z., C. Z. L. and H. W. carried out literature search, Y. X., S. Z. W. carried out manuscript editing, Y. L. H. and J. R. C. performed manuscript review. The authors declare no competing financial interest.

Conflicts of interest

There are no conflicts to declare.

Acknowledgements

References

1 G. Baffou and R. Quidant, Nanoplasmonics for Chemistry, *Chem. Soc. Rev.*, 2014, **43**, 3898–3907.

2 P. Christopher, H. Xin and S. Linic, Visible-Light-Enhanced Catalytic Oxidation Reactions on Plasmonic Silver Nanostructures, *Nat. Chem.*, 2011, **3**, 467–472.

3 J. Yang, Y. Li, L. Zu, L. Tong, G. Liu, Y. Qin and D. Shi, LightConcentrating Plasmonic Au Superstructures with Significantly Visible-Light-Enhanced Catalytic Performance, *ACS Appl. Mater. Interfaces*, 2015, **7**, 8200–8208.

4 U. Gunten, Ozonation of drinking water: part II. Disinfection and by-product formation in presence of bromide, iodide or chlorine, *Water Res.*, 2003, **37**, 1469–1487.

5 C. Zhang, M. Cao, H. Ma, C. Yu, K. Li, C. Yu and L. Jiang, Morphology-control strategy of the superhydrophobic soly (Methyl Methacrylate) surface for efficient bubble adhesion and wastewater remediation, *Adv. Funct. Mater.*, 2017, **27**, 1702020.

6 C. Yu, M. Cao, Z. Dong, K. Li, C. Yu, J. Wang and L. Jiang, Aerophilic electrode with cone shape for continuous generation and efficient collection of H2 bubbles, *Adv. Funct. Mater.*, 2016, **26**, 6830–6835.

7 P. Zhang, J. Zhang, Z. Xue, J. Wang and L. Jiang, Reliable manipulation of gas bubbles by regulating interfacial morphologies and chemical components, *Mater. Horiz.*, 2017, **4**, 665–672.

8 C. Yu, P. Zhang, J. Wang and L. Jiang, Superwettability of gas bubbles and its application: from bioinspiration to advanced materials, *Adv. Mater.*, 2017, **29**, 201703053.

9 H. Ma, M. Cao, C. Zhang, Z. Bei, K. Li, C. Yu and L. Jiang, Directional and continuous transport of gas bubbles on superaerophilic geometry-gradient surfaces in aqueous enviroments, *Adv. Funct. Mater.*, 2018, **28**, 1705091.

10 Y. Jiao, C. Li, S. Wu, Y. Hu, J. Li, L. Yang, D. Wu and J. Chu, Switchable Underwater Bubble Wettability on Laser-Induced Titanium Multiscale Micro-/Nanostructures by Vertically Crossed Scanning, *ACS Appl. Mater. Interfaces*, 2018, **10**, 16867–16873.

11 J. Yong, F. Chen, Y. Fang, J. Huo, Q. Yang, J. Zhang, H. Bian and X. Hou, Bioinspired design of underwater superaerophobic and superaerophilic surfaces by femtosecond laser ablation for anti- or capturing bubbles, *ACS Appl. Mater. Interfaces*, 2017, **9**, 39863–39871.

12 X. Tang, H. Xiong, T. Kong, Y. Tian, W. D. Li and L. Wang, Bioinspired Nanostructured Surfaces for On-Demand Bubble Transportation, *ACS Appl. Mater. Interfaces*, 2018, **10**, 3029–3038.

13 C. Yu, X. Zhu, M. Cao, C. Yu, K. Li and L. Jiang, Superhydrophobic helix: controllable and directional bubble transport in an aqueous environment, *J. Mater. Chem. A*, 2016, **4**, 16865.

14 M. Liu, S. Wang and L. Jiang, Nature-inspired superwettability systems, *Nat. Rev. Mater.*, 2017, **2**, 17036.

15 B. Su, Y. Tian and L. Jiang, Bioinspired interfaces with superwettability: from materials to chemistry, *J. Am. Chem. Soc.*, 2016, **138**, 1727–1748.

16 Y. Jiao, C. Li, X. Lv, Y. Zhang, S. Wu, C. Chen, Y. Hu, J. Li, D. Wu and J. Chu, In situ tunable bubble wettability with fast response induced by solution surface tension, *J. Mater. Chem. A*, 2018, **6**, 20878–20886.

17 J. Yong, F. Chen, M. Li, Q. Yang, Y. Fang, J. Huo and X. Hou, Remarkably simple achievement of superhydrophobicity, superhydrophilicity, underwatersuperoleophobicity, underwater superoleophilicity, underwater superaerophobicity, and underwater superaerophilicity on femtosecond laser ablated PDMS surfaces, *J. Mater. Chem. A*, 2017, **5**, 25249–25257.

18 C. Yu, X. Zhu, K. Li, M. Cao and L. Jiang, Manipulating bubbles in aqueous environment via a lubricant-infused slippery surface, *Adv. Funct. Mater.*, 2017, **27**, 201701605.

19 C. Shi, X. Cui, X. Zhang, P. Tchoukov, Q. Liu, N. Encinas, M. Paven, F. Geyer, D. Vollmer, Z. Xu, H. J. Butt and H. B. Zeng, Interaction between air bubbles and superhydrophobic surfaces in aqueous solutions, *Langmuir*, 2015, **31**, 7317–7327.

20 L. Xie, C. Shi, X. Cui and H. B. Zeng, Surface forces and interaction mechanisms of emulsion drops and gas bubbles in complex fluids, *Langmuir*, 2017, **33**, 3911–3925.

21 C. Zhang, B. Zhang, H. Ma, Z. Li, X. Xiao, Y. Zhang, X. Cui, C. Yu, M. Cao and L. Jiang, Bioinspired Pressure-Tolerant Asymmetric Slippery Surface for Continuous Self-Transport of Gas Bubbles in Aqueous Environment, *ACS Nano*, 2018, **12**, 2048–2055.

22 C. Pei, Y. Peng, Y. Zhang, D. Tian, K. Liu and L. Jiang, An Integrated Janus Mesh: Underwater Bubble Anti-Buoyancy Unidirectional Penetration, *ACS Nano*, 2018, **12**, 5489–5494.

23 T. S. Wong, S. H. Kang, S. K. Y. Tang, E. J. Smythe, B. D. Hatton, A. Grinthal and J. Aizenberg, Bioinspired self-repairing slippery surfaces with pressure-stable omniphobicity, *Nature*, 2011, **477**, 443–447.

24 J. C. Loudet, P. Hanusse and P. Poulin, Stokes drag on a sphere in a nematic liquid crystal, *Science*, 2004, **306**, 1525–1525.

25 J. Masliyah, R. Jauhari and M. Gray, Drag coefficients for air bubbles rising along an inclined surface, *Chem. Eng. Sci.*, 1994, **49**, 1905–1911.

26 P. G. De Gennes, Wetting, statics and dynamics, *Rev. Mod. Phys.*, 1985, **57**, 827.

27 D. Bonn, J. Eggers, J. Indekeu, J. Meunier and E. Rolley, Wetting and spreading, *Rev. Mod. Phys.*, 2009, **81**, 739.

28 X. Cui, J. Liu, L. Xie, J. Huang, Q. Liu, J. N. Israelachvili and H. B. Zeng, Modulation of Hydrophobic Interaction by Mediating Surface Nanoscale Structure and Chemistry, not Monotonically by Hydrophobicity, *Angew. Chem., Int. Ed.*, 2018, **57**, 11903–11908.